International Journal of Heat and Mass Transfer 120 (2018) 350–360

Contents lists available at ScienceDirect

International Journal of Heat and Mass Transfer

journal homepage: www.elsevier.com/locate/ijhmt

# Finite element analysis of self-excited instabilities in a lean premixed gas turbine combustor

Seong-Ku Kim [a], Daesik Kim [b,*], Dong Jin Cha [c]

[a] Combustion Chamber Team, Korea Aerospace Research Institute, 169-84 Gwahak-ro, Yuseong-gu, Daejeon 305-806, Republic of Korea
[b] Department of Precision Mechanical Engineering, Gangneung-Wonju National University, 150 Namwon-ro, Wonju-si, Gangwon-do 220-711, Republic of Korea
[c] Department of Building and Plant Engineering, Hanbat National University, 125 Dongseodae-ro, Yuseong-gu, Daejeon 305-719, Republic of Korea

ARTICLE INFO

*Article history:*
Received 2 April 2017
Received in revised form 6 November 2017
Accepted 5 December 2017
Available online 18 December 2017

*Keywords:*
Combustion instability
Thermoacoustics
Helmholtz solver
Flame transfer function
Reflection coefficient

ABSTRACT

The present study numerically simulates self-excited instabilities of hydrogen-blended natural gas flames in a lean premixed gas turbine combustor with variable chamber length. In order to effectively predict the thermoacoustic instability within the detailed geometry of the combustor, the Helmholtz equation is discretized with a Galerkin finite element method on a three-dimensional hybrid unstructured mesh. The unsteady heat release rate is modeled with an experimentally measured flame transfer function. The nonlinearity associated with the flame response term is handled with an iterative method, and the large-scale eigenvalue problem is solved by means of the shift-invert method of the ARPACK (ARnoldi PACKage) software. The present Helmholtz solver reproduces the experimentally observed instabilities in terms of the mode frequency and the chamber length range of self-excited pressure oscillations which are significantly affected by the hydrogen enrichment of natural gas fuel. The effects of the acoustic boundary condition and the flame response model on the predictive accuracy are also discussed.



## 1. Introduction

Lean premixed combustion technology has been widely utilized in modern gas turbine engines because of its ability to simultaneously reduce NOx emissions and achieve high fuel consumption efficiency. However, lean premixed combustors are highly susceptible to self-excited pressure oscillations [1]. The phenomenon known as combustion instability results from a feedback coupling between the unsteady heat release and the acoustic waves formed resonantly in the combustion system [2,3]. This thermoacoustic instability is frequently accompanied by large-amplitude mechanical vibrations and excessive heat transfer to the hardware [4].

Although much effort has been devoted to dealing with the fundamental and practical issues associated with combustion instabilities in low-emission gas turbines during the last three decades, the complex phenomena involving turbulent flow, chemical kinetics, flame dynamics, and their interactions with acoustics are not yet fully understood [5]. Furthermore, there has been a strong need for reliable numerical tools to predict combustion instabilities at the design level in order to reduce costly and time-consuming trial-and-error loops in the development of advanced gas turbines [6].

The numerical methods to predict combustion instabilities can be classified depending on the degree of the assumptions and simplifications used in solving the thermoacoustic problems. For the lowest order method, the combustor can be modeled simply as a network of homogeneous acoustic elements that are represented individually through one-dimensional analytical solutions and connected to one another by enforcing jumping relations [7]. Although this lumped element network model has been effectively used for either fundamental research [8] or preliminary design purposes [9], its crude approximations lead to some severe limitations. In this model, geometrical details cannot be taken into account, and only the equivalent longitudinal or orthoradial modes are calculated. Moreover, the flame is assumed to be infinitely thin, and its response to the incident acoustic perturbations must be modeled in a simplified manner.

In contrast, the LES (Large Eddy Simulation) technique has evolved enough to correctly capture the essential physics underlying the combustion instabilities [10,11]. Many recent studies have demonstrated its ability to simulate the combustion dynamics of turbulent premixed flames [12,13]. From a practical point of view, however, the computational cost is still too high to apply the LES to an actual combustor design.

As a reasonable compromise between high fidelity and low cost, a Helmholtz solver called AVSP [14] has been developed by researchers at CERFACS and the University of Montpellier. In order

* Corresponding author.
*E-mail address:* dkim@gwnu.ac.kr (D. Kim).

https://doi.org/10.1016/j.ijheatmasstransfer.2017.12.021
0017-9310/

to solve the thermoacoustic problem, Nicoud et al. [14] proposed a new numerical procedure in which a three-dimensional Helmholtz equation coupled with the time-lag hypothesis is discretized with a finite element method (FEM), and the stability characteristics of the system are predicted in terms of the resonant frequencies and amplification rates for all possible acoustic modes by solving a nonlinear eigenvalue problem. The AVSP code has been used in combination with a compressible reacting LES code to study the flame-acoustic coupling mechanisms in laboratory-scaled premixed swirl burners [15,16] and to provide stability maps for azimuthal modes in the full annular combustor of a real helicopter engine [17]. Gullaud and Nicoud [18] have devised an analytical model to describe the acoustic behavior of a multiperforated plate and implemented it into the AVSP code to account for the effects of cooling holes on aeronautical gas turbine combustion chamber walls. Silva et al. [19] have developed a numerical method based on one-dimensional LEE (Linearized Euler Equations) to define acoustic boundary impedances that can be used as upstream and downstream flow boundary conditions for the AVSP code. These boundary conditions are relevant to the rotor stages of the compressors and turbines. Consequently, although the flame-acoustic interactions must be modeled in a simplified manner, the Helmholtz solver has several advantages because it accounts for three-dimensional geometrical details, spatial distributions of the flame parameters, and frequency-dependent boundary impedances with much less computational cost than the LES approach. A comparative overview of the available methods for predicting thermoacoustics in combustors is presented in the previous work of Nicoud et al. [14].

Remarkable progress has been achieved in the recent work of Silva et al. [20]. To predict the limit cycle behaviors of the combustion instabilities primarily associated with the nonlinearity of flame dynamics, they have combined the AVSP code with measured flame describing functions in which the nonlinear flame responses are represented not only by the frequency of the incoming velocity perturbation but also by their amplitude in a swirled premixed combustor. The amplitude and frequency of the limit cycles have been numerically determined by equating the predicted growth rate to the measured damping of the system. The results were in reasonable agreement with the experimental observations.

Another approach to the Helmholtz solver was attempted by Camporeale et al. [21]. In their work, the numerical procedure of Nicoud et al. [14] was embodied in a commercial FEM software, COMSOL Multiphysics, and validated successfully against several benchmark cases available in the literature. Their Helmholtz solver framework has recently been combined with nonlinear polynomial flame response models to investigate the supercritical and subcritical bifurcation processes of self-sustained pressure oscillations in a simple longitudinal combustor and an annular combustion chamber [22].

It is also worthwhile to pay attention to another hybrid methodology of CFD (Computational Fluid Dynamics) and CAA (Computational Aero-Acoustics), in which a frequency-domain simulation of LEE (Linearized Euler Equations) or LNSE (Linearized Navier-Stokes Equations) is employed instead of the Helmholtz equation. Very recently, Ullrich et al. [23] have performed the LNSE simulations with the mean flowfield and noise source term determined by RANS and LES to predict complex combustion noise of a lean-premixed, swirled combustor. Similarly, the LEE simulations with flame response models have been applied for linear stability analysis of high-frequency transverse modes in a gas turbine combustor [24] as well as a cryogenic rocket combustion chamber [25].

The previous studies have fully demonstrated that the Helmholtz solver framework can be utilized as a promising tool for both academic research and industrial design purposes in combination with the LES calculation and experimental measurements. Despite its high potential, however, the Helmholtz solvers (i.e., the in-house code (AVSP) and the commercial FEM application (COMSOL)) have been developed and utilized only by the aforementioned research groups until now. It would be desirable for this new methodology to be spread widely throughout the research and industrial fields and, also, further verified and improved through various applications.

In this context, the present study was designed to construct a Helmholtz solver with reference to the previous work of Nicoud et al. [14]. In order to improve numerical efficiency and robustness, the in-house code, ASCI3D (Acoustic Solver for Combustion Instability in 3-Dimension), adopts a three-dimensional FEM on a mixed element mesh consisting of hexahedral, pyramidal, prismatic, and tetrahedral elements [26]. ASCI3D uses the shift-invert method available in the ARPACK (ARnoldi PACKage) library [27] for solving the large-scale eigenvalue problem. In this study, the ASCI3D code is applied to numerically investigate self-excited instabilities in a lean premixed gas turbine combustor with well-established measurements, conducted by Kim et al. [28–30], that have not yet been analyzed with the Helmholtz solver framework. The flame-acoustic interaction is modeled through the measured flame transfer functions for two different flame conditions. The present study focuses on the ability of the Helmholtz solver to predict experimentally observed instability ranges for chamber length, which vary significantly depending on the flame conditions. In addition, we discuss which part of the flame response model plays a crucial role and how the acoustic condition at the inflow boundary affects the mode shape and acoustic loss. These discussions point to further research directions for improving predictive accuracy.

## 2. Numerical methodology

The numerical methodology used in the present study is mainly based on the aforementioned works of Nicoud and his colleagues. Therefore, we describe briefly the mathematical formulations and numerical methods that are necessary to explain the structure of our in-house Helmholtz solver and the modeling issues of interest in this study. Further details can be found elsewhere [14–16,20,31].

### 2.1. Mathematical formulations

In the linear acoustic analyses, all the physical quantities are assumed to oscillate harmonically at a complex valued angular frequency. By assuming harmonic variation, the pressure fluctuation, for example, can be expressed as [14]

$$p'(\mathbf{x},t) = \mathrm{Re}\{\hat{p}(\mathbf{x})\mathrm{e}^{-i\omega t}\} = \mathrm{Re}\{\hat{p}(\mathbf{x})\mathrm{e}^{-i\omega_r t}\}\ \mathrm{e}^{\omega_i t} \tag{1}$$

where the hat ($\wedge$) over a variable indicates the Fourier transformation, and $\omega$ denotes the complex angular frequency ($\omega = \omega_r + i\omega_i$). The acoustic pressure field is composed of three parts: (1) the complex pressure field, $\hat{p}(\mathbf{x})$, which represents an acoustic mode and is a spatial function independent of time; (2) the real part of the complex angular frequency which yields the resonant frequency (i.e., $f = \omega_r/(2\pi)$); and (3) the imaginary part $\omega_i$, which determines the growth rate of the pressure oscillation. As can be seen in Eq. (1), if it is positive ($\omega_i > 0$), the amplitude of the oscillations increases exponentially with time. On the other hand, a negative value means that the oscillations are damped out.

Under the above assumptions, the linear wave equation for a low Mach number reacting flow in a non-dissipation medium can be transformed into the Helmholtz equation in the frequency domain as follows:

$$\nabla \cdot \left(\frac{1}{\rho_0}\nabla \hat{p}\right) + \frac{\omega^2}{\gamma p_0}\hat{p} = i\omega\frac{\gamma - 1}{\gamma p_0}\hat{q} \tag{2}$$

where $\hat{q}$ is the complex amplitude of the heat release fluctuation for a given combustion system and must be modeled to close the thermoacoustic problem (as is explained in Section 2.2). The complete derivation of the Helmholtz equation can be found elsewhere [14,16], and is not repeated here. By solving the eigenvalue problem resulting from the Helmholtz equation of Eq. (2), the eigenfrequency $\omega$ and eigenfunction $\hat{p}(\mathbf{x})$ allow one to identify the acoustic mode shape, the resonance frequency, and the onset of the thermoacoustic instability previously mentioned in Eq. (1).

To generalize the boundary conditions for the Helmholtz equation, a reduced acoustic impedance is introduced as

$$Z = \frac{\hat{p}}{\rho_0 c_0(\hat{\mathbf{u}} \cdot \mathbf{n}_{\mathrm{bc}})} \tag{3}$$

where $\mathbf{n}_{\mathrm{bc}}$ denotes the outward unit normal vector to the boundary surface. The impedance $Z$, is given as a complex-valued function of $\omega$, depending on the physical features of the acoustic boundaries [32]. As a simple example, the impedance has an infinite value ($Z \to \infty$) at perfectly reflecting boundaries, such as a rigid wall ($\hat{\mathbf{u}} \cdot \mathbf{n}_{\mathrm{bc}} = 0$). For an outlet at constant pressure ($\hat{p} = 0$), $Z = 0$. On the other hand, for non-reflecting boundary conditions, such as an infinitely long duct, $Z = 1$.

### 2.2. Flame response modeling

Modeling the flame response to the acoustic perturbations is the key mechanism for the Helmholtz solver with respect to predicting the thermoacoustic instabilities. For the premixed flames, a velocity-sensitive time lag hypothesis has generally been employed to link the unsteady heat release oscillations with the upstream velocity perturbations.

$$\frac{q'(\mathbf{x},t)}{q_{\mathrm{tot}}} = n(\mathbf{x})\frac{\mathbf{u}'(\mathbf{x}_{\mathrm{ref}}, t - \tau(\mathbf{x})) \cdot \mathbf{n}_{\mathrm{ref}}}{u_{\mathrm{bulk}}} \tag{4}$$

Here, $n(\mathbf{x})$ denotes a local interaction index, and $\tau(\mathbf{x})$ represents a local time delay between the local heat release oscillation, $q'(\mathbf{x},t)$, and the incoming velocity perturbation at a reference location, $\mathbf{u}'(\mathbf{x}_{\mathrm{ref}}, t)$. The reference values of heat release rate and velocity, $q_{\mathrm{tot}}$ and $u_{\mathrm{bulk}}$, are used as scaling factors for the dimensionless interaction index, $n(\mathbf{x})$. The two model parameters, $n$ and $\tau$, are determined by the physical mechanisms underlying the flame dynamics, and they can be quantified by experimental measurement or by a LES of the reacting flow.

Consistent with the Helmholtz equation, the flame response model of Eq. (4) can be transformed into the frequency domain as

$$\hat{q}(\mathbf{x}) = \frac{q_{\mathrm{tot}}}{u_{\mathrm{bulk}}} n(\mathbf{x}) e^{i\omega\tau(\mathbf{x})}\hat{\mathbf{u}}(\mathbf{x}_{\mathrm{ref}}) \cdot \mathbf{n}_{\mathrm{ref}} \tag{5}$$

Assuming a low Mach number flow, the complex acoustic velocity can be obtained with the divergence of the complex pressure through the following linearized momentum equation [14,15]:

$$\hat{\mathbf{u}} = \frac{\nabla \hat{p}}{i\omega\rho_0} \tag{6}$$

By substituting Eq. (6) into Eq. (5), the complex amplitude of the heat release rate can be obtained in the following form to close the Helmholtz equation of Eq. (2):

$$\hat{q}(\mathbf{x}) = \frac{q_{\mathrm{tot}}}{i\omega\rho_{\mathrm{ref}}u_{\mathrm{bulk}}} n(\mathbf{x}) e^{i\omega\tau(\mathbf{x})}\nabla\hat{p}(\mathbf{x}_{\mathrm{ref}}) \cdot \mathbf{n}_{\mathrm{ref}} \tag{7}$$

### 2.3. Numerical method

In this study, to effectively resolve the complex geometry of actual combustors, the computational domain is divided into a mixed element mesh consisting of hexahedra, pyramids, prisms, and tetrahedra. The complex acoustic pressure field is approximated by discrete values $\hat{p}_\beta$ at the vertices with a piecewise linear shape function $\phi_\beta$. The Helmholtz equation from Eq. (2), coupled with the flame response model from Eq. (7), is spatially discretized with a classical Galerkin finite element method, resulting in a nonlinear eigenvalue problem as follows:

$$A_{\alpha\beta}\hat{p}_\beta + \omega B_{\alpha\beta}\hat{p}_\beta + \omega^2 C_{\alpha\beta}\hat{p}_\beta = D_{\alpha\beta}(\omega)\hat{p}_\beta \tag{8}$$

Here, the coefficient matrices are given as follows:

$$A_{\alpha\beta} = -\int_\Omega \frac{1}{\rho_0}\frac{\partial\phi_\alpha}{\partial x_i}\frac{\partial\phi_\beta}{\partial x_i}d\Omega + \int_{\partial\Omega_Z}\frac{i}{\rho_0 c_0}Z_2\phi_\alpha^*\phi_\beta d\Gamma \tag{9}$$

$$B_{\alpha\beta} = \int_{\partial\Omega_Z}\frac{i}{\rho_0 c_0}\frac{1}{Z_0}\phi_\alpha^*\phi_\beta d\Gamma \tag{10}$$

$$C_{\alpha\beta} = \int_\Omega \frac{1}{\gamma p_0}\phi_\alpha\phi_\beta d\Omega + \int_{\partial\Omega_Z}\frac{i}{\rho_0 c_0}Z_1\phi_\alpha^*\phi_\beta d\Gamma \tag{11}$$

$$D_{\alpha\beta}(\omega) = \int_\Omega \frac{\gamma - 1}{\gamma p_0}\frac{q_{\mathrm{tot}}}{\rho_{\mathrm{ref}}u_{\mathrm{bulk}}}n(\mathbf{x})e^{i\omega\tau(\mathbf{x})}\phi_\alpha\nabla\phi_\beta(\mathbf{x}_{\mathrm{ref}}) \cdot \mathbf{n}_{\mathrm{ref}}d\Omega \tag{12}$$

It should be noted that the contributions of the boundary conditions are separately contained in the coefficient matrices $A_{\alpha\beta}, B_{\alpha\beta}$, and $C_{\alpha\beta}$ from Eqs. (9)–(11) by assuming that the dependence of the boundary impedance, $Z$, on the complex angular frequency, $\omega$, takes the following form [14,15]:

$$\frac{1}{Z} = \frac{1}{Z_0} + Z_1\omega + \frac{Z_2}{\omega} \tag{13}$$

Numerical difficulty in solving Eq. (8) is caused by the nonlinear source term $D_{\alpha\beta}$ in which the flame response parameters $n$ and $\tau$ are determined implicitly by the eigenfrequency $\omega$. The nonlinearity is handled by an iterative method [14], and the flame response term is linearized with the latest update of $\omega_{k-1}$ at the $k$th iteration as follows:

$$\left[A_{\alpha\beta} - D_{\alpha\beta}(\omega_{k-1})\right]\hat{p}_\beta + \omega_k B_{\alpha\beta}\hat{p}_\beta + \omega_k^2 C_{\alpha\beta}\hat{p}_\beta = 0 \tag{14}$$

By doing so, Eq. (8) is simplified into a quadratic eigenvalue problem which depends only on $\omega$ and $\omega^2$ in the following form:

$$\mathbf{A}_0\mathbf{P} + \omega\mathbf{B}_1\mathbf{P} + \omega^2\mathbf{C}_2\mathbf{P} = 0 \tag{15}$$

The quadratic eigenvalue problem from Eq. (15) can be straightforwardly converted into a generalized eigenvalue problem as follows:

$$\mathbf{A}^*\mathbf{x} = \omega\mathbf{B}^*\mathbf{x} \tag{16}$$

where

$$\mathbf{A}^* = \begin{bmatrix} -\mathbf{B}_1 & -\mathbf{A}_0 \\ \mathbf{I} & \mathbf{0} \end{bmatrix}, \quad \mathbf{B}^* = \begin{bmatrix} \mathbf{C}_2 & \mathbf{0} \\ \mathbf{0} & \mathbf{I} \end{bmatrix}, \quad \mathbf{x} = \begin{bmatrix} \omega\mathbf{P} \\ \mathbf{P} \end{bmatrix} \tag{17}$$

The generalized large-scale eigenvalue problem from Eq. (16) is solved with the Implicitly Restarted Arnoldi method [27]. To enhance the computational efficiency when solving the eigenvalue problem, the present study uses the shift-invert method in which the standard form of Eq. (16) is converted into the following equation with the shift $\sigma$:

$$(\mathbf{A}^* - \sigma\mathbf{B}^*)^{-1}\mathbf{B}^*\mathbf{x} = \frac{1}{\omega - \sigma}\mathbf{x} \tag{18}$$

The shift-invert method yields better performance than the standard method of handling Eq. (16) directly. Moreover, while the

standard method requires sequential calculation of all the eigenmodes, starting from the lowest eigenfrequency to the frequency of interest, the shift-invert method requires the calculation of only the desirable number of eigenmodes (i.e., those existing in the vicinity of a target frequency which is prescribed by the shift $\sigma$). However, the shift-invert method has a numerical drawback. As the shift $\sigma$, approaches the eigenvalue $\omega$, the complex-valued matrix $(\mathbf{A}^* - \sigma\mathbf{B}^*)$ becomes singular, and it would be difficult for its inversion to converge, even with state of the art iterative matrix solvers. In this study, to enforce the convergence and robustness, the complex-valued linear system is solved with the MUMPS (MUltifrontal Massively Parallel sparse direct Solver) [33,34].

Fig. 1 schematically summarizes the overall solution procedure that has been implemented into our in-house Helmholtz solver ASCI3D, which is written in Fortran 90.

## 3. Results and discussion

### 3.1. Validation case: thin flat premixed flame

First, to validate the present Helmholtz solver ASCI3D, with respect to numerical aspects, we solve an ideal problem. This problem assumes an infinitely thin flat premixed flame with a theoretical solution, against which the AVSP code has already been validated during initial development [14]. As shown in Fig. 2, the inlet on the left side is acoustically closed ($Z = \infty$), and the exit on the right side is assumed to be open into a large space ($Z = 0$). Because of the passive effect of the infinitely thin flat premixed flame located at the center, the gas properties are abruptly changed to the left and to the right of the flame. There exists a theoretical solution in accordance with the matching conditions on the left and right sides of the flame surface [14]. In this study, the computational domain is divided into a hybrid mesh consisting of 16,320 hexahedral and 17,952 prism elements with the grid spacing clustered axially near the flame. The infinitely thin flame thickness is approximated numerically by two element spacings of 0.4 mm, which corresponds to 0.08% of the axial length of the computational domain. The flame response is modeled with the velocity-sensitive time lag model from Eq. (7).

Fig. 3 presents the comparison between the numerical and theoretical solutions in terms of the resonant frequency and the growth rate for two values of global interaction index $\bar{n}$, 0.01 and 5.0, and a constant time delay $\tau$, of 0.1 ms. The results of the complex-valued eigenfrequencies can be interpreted to have a physical meaning as follows: the third longitudinal (3L) mode causes a thermoacoustic instability near 1200 Hz for the given time delay ($\tau = 0.1$ ms), and an increase in the global interaction index leads to more rapidly amplified oscillations at a slightly higher resonant frequency. For all the eigenmodes, the numerical results agree very well with the theoretical solutions. With respect to the iteration method used to handle the nonlinearity of the flame response term, the complex eigenfrequency of the 3L mode with $\bar{n} = 5.0$ was converged at four iterations with a stopping criterion of $|\omega_k - \omega_{k-1}|/|\omega_0| < 10^{-4}$.

### 3.2. A lean premixed swirl-stabilized gas turbine combustor

Next, we numerically simulated self-excited pressure oscillations in the lean premixed swirl-stabilized gas turbine combustor used by Kim et al. [28–30], which is illustrated schematically in Fig. 4(a). The model combustor consists of a removable siren, a mixing section with a flat vane swirler, an optically-accessible quartz combustor section, a variable length steel combustion chamber, and an exhaust section. Although it has a relatively sim-

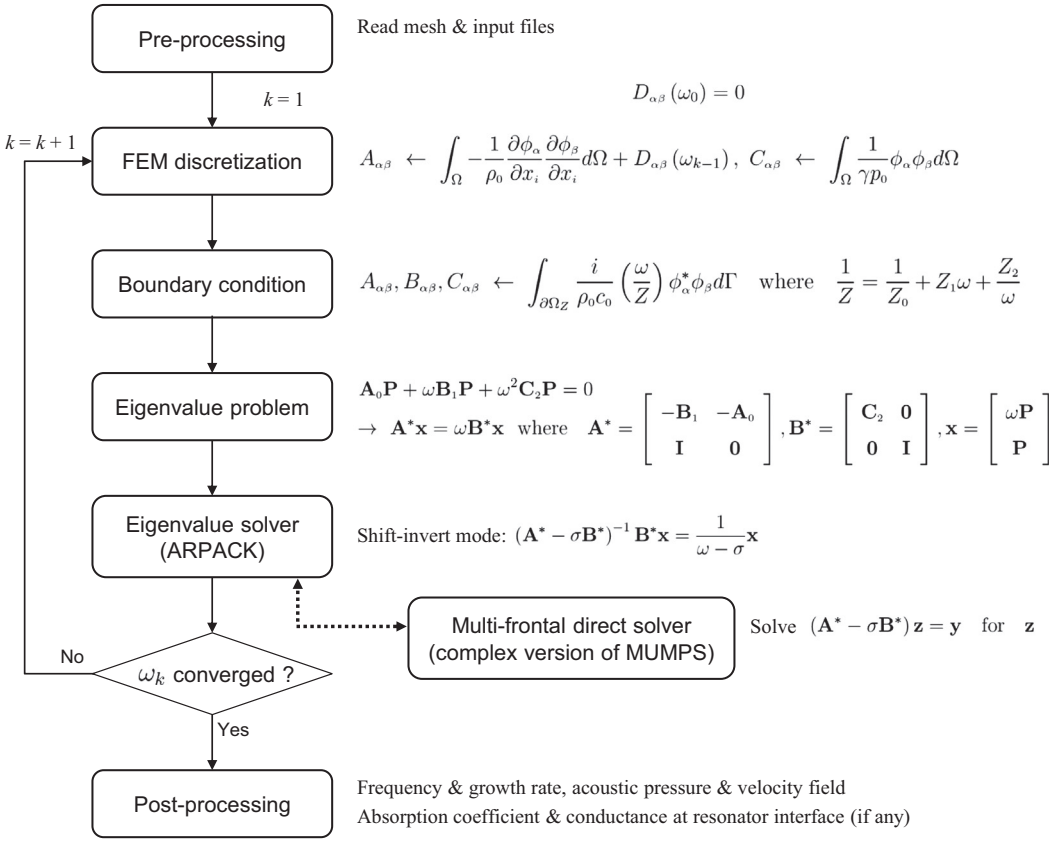


**Fig. 1.** Solution procedure for the Helmholtz solver ASCI3D.

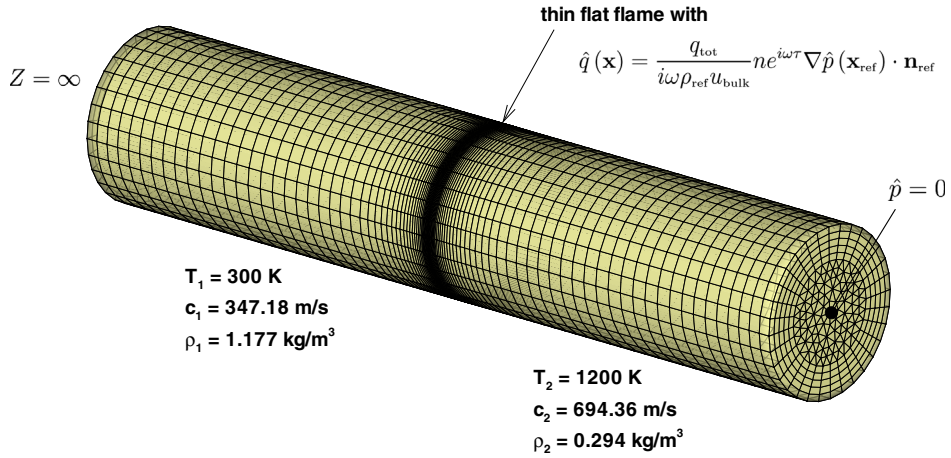


**Fig. 2.** Computational mesh for coupling between a thin flat premixed flame and longitudinal acoustic modes.

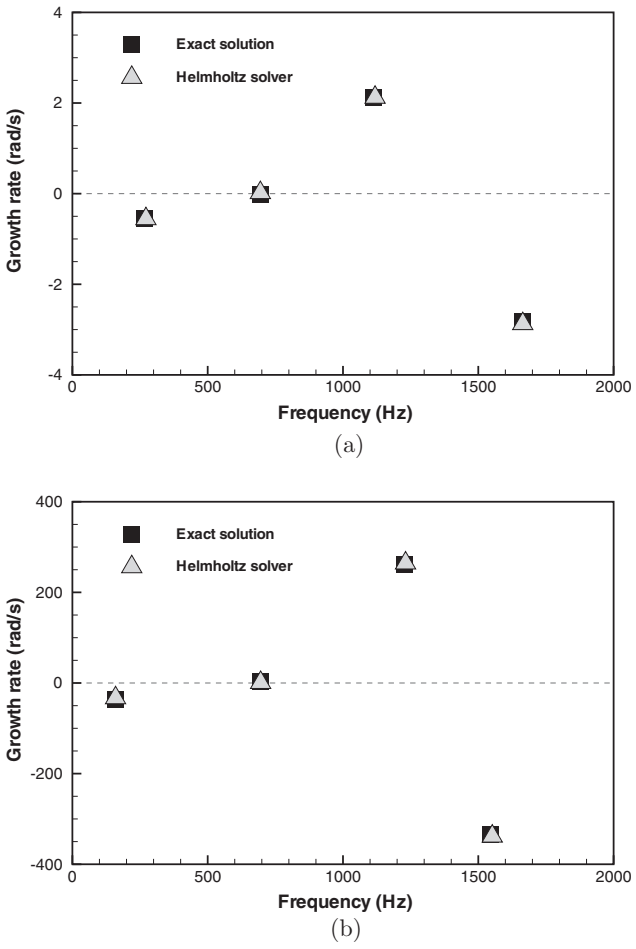


**Fig. 3.** Comparison of eigenfrequencies between theoretical and numerical solutions for (a) global interaction index $\bar{n} = 0.01$ and (b) $\bar{n} = 5.0$.

ple geometry, the combustor has been devised to represent the turbulent flame dynamics encountered in real gas turbine combustors. Hydrogen-blended natural gas is injected and mixed with preheated air upstream of the choked inlet to ensure that the reactant mixtures are spatially and temporally homogeneous before entering the combustion chamber. The total length of the combustion chamber can be continuously varied from 762 mm to 1524 mm. For the forced flame response measurements, a siren type modulation device is mounted to generate inlet velocity fluctuations at a forcing frequency ranging from 100 Hz to 400 Hz. The dynamic responses of the turbulent premixed flame to the forcing acoustic modulations were characterized qualitatively through chemiluminescence emissions and measured quantitatively in terms of the flame transfer function. In addition, spontaneous instability regimes were determined in terms of the combustion chamber lengths when self-excited pressure oscillations were observed without the siren. The experimental results demonstrated that the amount of hydrogen added to the natural gas fuel has a substantial impact on the flame behaviors and the subsequent instability characteristics. Considering the detailed measurement data, as well as the well-defined geometry and flame conditions, these results can serve to validate the predictive capability of the Helmholtz solver.

Fig. 4(b) shows the mesh system consisting of 55,272 hexahedral elements and 62,519 node points. For the purposes of calculation efficiency, since only the longitudinal acoustic modes are of interest to this study, only a 45° sector in the circumferential direction is selected for the computational domain. The same boundary conditions as those used in the acoustic analysis with the lumped element network model by Kim et al. [30], are imposed on the flow boundaries in the present simulations. The inlet boundary condition is determined with the reflection coefficient measured during self-excited oscillations ($R_{in}$ = 0.2292–0.1894$i$) [30]. The reflection coefficient $R$ is measured as the ratio of the reflection wave to the incident wave and converted to the reduced impedance $Z$, using the relation of $Z = (1 + R)/(1 - R)$. Since the combustor outlet is restricted by a plug with a blockage ratio of about 80%, it is assumed to be acoustically closed ($R_{out} = 1$). In the thermoacoustic problem, the acoustic boundary condition has a critical impact on the mode shape of the pressure oscillations and, subsequently, on the feedback coupling with the heat release fluctuations [35,36]. The effect of the inlet boundary condition on the spontaneous instability characteristics will be discussed later.

Two different flame conditions, which are hereafter denoted as Flame H00 (pure natural gas fuel) and Flame H45 (45% $H_2$ addition), are summarized in Table 1. The experimental work of Kim et al. [28] revealed that the variations in the fuel compositions have a significant impact on the flame structure and the flame attachment points. As illustrated in Fig. 5, Flame H00 exhibits an enveloped "M" flame with a non-compact shape, whereas Flame H45 yields a dihedral "V" flame with a relatively shortened length. The flame structure is one of the key parameters determining the flame response to acoustic and convective perturbations. In the present simulation, the flame region is approximated from the

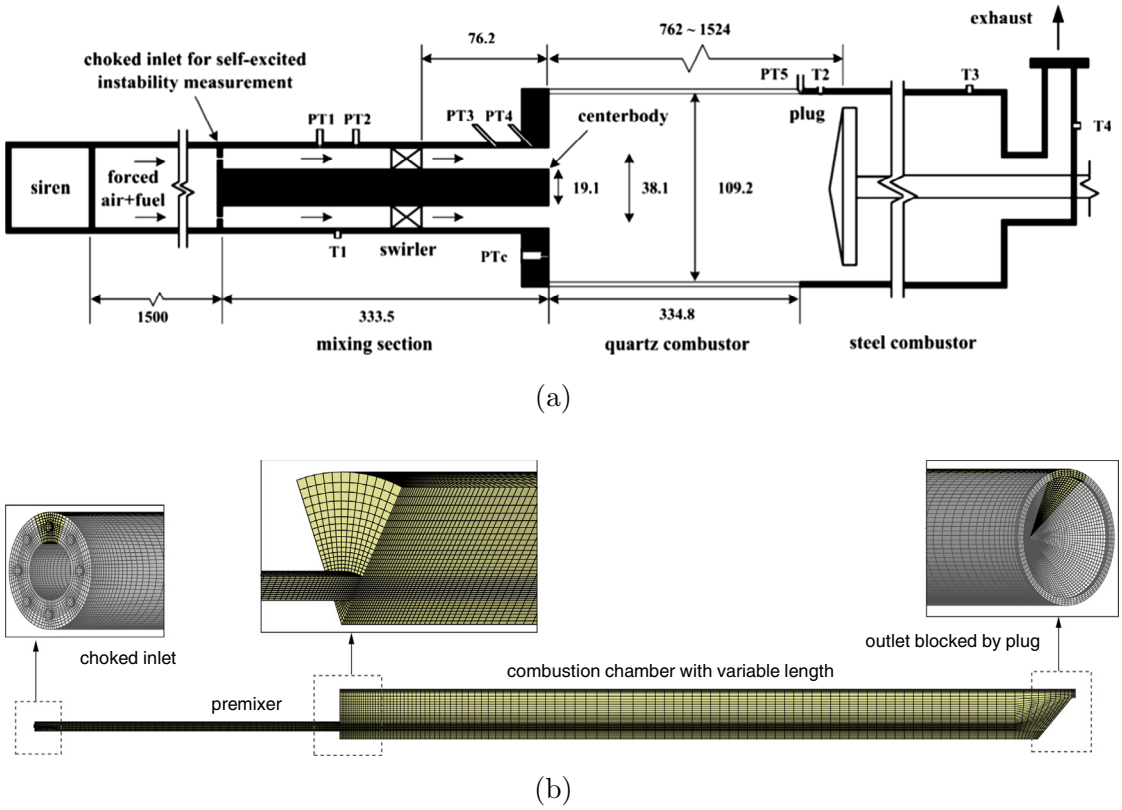


**Fig. 4.** Swirl-stabilized, lean-premixed, gas turbine combustor. (a) Experimental setup with dimensions in millimeters (reproduced from [30] with the author's permission); (b) Computational mesh.

**Table 1**
Two different flame conditions of the lean premixed gas turbine combustor.

| Flame condition | Flame H00 | Flame H45 |
|---|---|---|
| Fuel molar composition | 100% natural gas | 55% natural gas + 45% $H_2$ |
| Equivalence ratio | 0.6 | 0.6 |
| Inlet temperature (K) | 473 | 473 |
| Reference velocity (m/s) | 60 | 60 |
| Thermal power (kW) | 62.9 | 91.6 |
| Operating pressure (atm) | 1 | 1 |
| Chamber length (m) | 0.8–2.0 | 0.8–2.0 |

measured flame image, as shown in Fig. 5. The local interaction index from Eq. (7) is set to zero everywhere except within the modeled flame region. In addition to the actual flame shape model, the thin flat flame model is used for comparative calculations to assess the effects of the flame shape on the predictive accuracy.

Essentially, the flame acts as both a passive and an active element in the thermoacoustic system. The former has an influence on the system through changes in the gas property distribution caused by turbulent combustion processes occurring in the flame region. The thermochemical properties of the unburnt reactant mixture and the combustion gas required for the Helmholtz solver are listed in Table 2. The combustion gas properties are obtained by chemical equilibrium calculations for the flame conditions given in Table 1. With respect to the gas properties, the computational domain is divided into two simple parts, the mixing section (unburnt mixture) and the combustion chamber (burnt gas), each of which is assumed to have a uniform distribution of gas properties, regardless of the flame shape.

As an active element in the thermoacoustic system, the flame responds interactively with the acoustic and convective perturbations. In order to quantify the response of premixed flames, the FTF (Flame Transfer Function) is defined as the combination of the heat release rate fluctuation $\hat{Q}$, and the incoming velocity perturbation $\hat{u}$ as follows:

$$FTF(\omega) = \frac{\hat{Q}/\bar{Q}}{\hat{u}/\bar{u}} = G(\omega)e^{i\phi(\omega)} \tag{19}$$

where $\bar{Q}$ and $\bar{u}$ denote the reference values for flame power and incoming velocity, respectively, and are used for scaling purposes. The gain $G$ and the phase delay $\phi$ are given as functions of frequency and must be either measured experimentally or extracted from a numerical simulation. Because of the similarity between the sensitive time-lag model from Eq. (7) and the FTF from Eq. (19), the model parameters $n$ and $\tau$ can be related directly to the gain $G$ and the phase delay $\phi$, respectively [31]. The present calculations use the global FTF measurements which are given as functions of frequency for the two flame conditions, as shown in Fig. 6. It should be noted that the global FTF describes a representative behavior for the whole flame and therefore, cannot take into account the spatial distribution of the unsteady heat release that could play a crucial role in the case of non-compact flames. In addition to the global FTF measurements, Kim et al. [30] also measured the longitudinal distributions of the FTF in the model combustor and revealed that the local convective time delay $\tau$ increases almost linearly with the axial distance within the flame region. This agrees with the analytical model of Armitage et al. [37], in which the distribution of time delay is assumed to be distributed linearly between $\tau - \Delta\tau$ and $\tau + \Delta\tau$. In the present study, therefore, the axial profile of time delay is modeled as a linear function with a range of $\tau \pm \Delta\tau$ within the actual flame shape given in Fig. 5. The value at the center, $\tau$ is obtained from the global FTF measurement shown in Fig. 6. With respect to the spatial deviation, $\Delta\tau/\tau$ is presumed to be 80% and

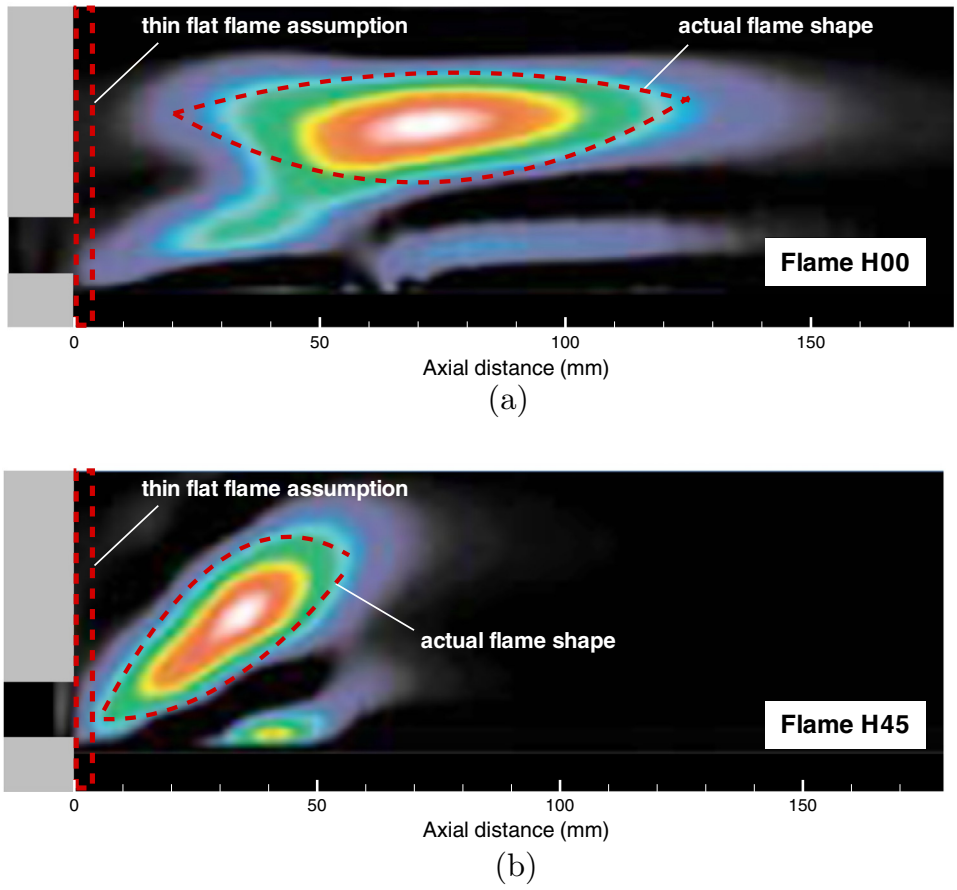


**Fig. 5.** Flame shape modeling based on stable flame images measured for (a) Flame H00 and (b) Flame H45 [28].

**Table 2**
Gas properties used in the calculation of the Helmholtz solver for the two flame conditions.

| Flame condition | Flame H00 | | Flame H45 | |
|---|---|---|---|---|
| Gas properties | Unburnt mixture | Burnt gas | Unburnt mixture | Burnt gas |
| Density (kg/m$^3$) | 0.7231 | 0.1913 | 0.7005 | 0.1858 |
| Specific heat ratio | 1.3705 | 1.2614 | 1.3734 | 1.2590 |
| Speed of sound (m/s) | 438.2 | 817.5 | 445.7 | 828.6 |

50% for Flame H00 and Flame H45, respectively, based on the local convective time measurements (see also Figs. 9 and 10 of Ref. [30]).

In order to examine the aforementioned modeling issues, four different calculations are carried out and compared, as listed in Table 3. The baseline model, denoted as Model A, is thought to be the best modeling combination available in the present study. Model B differs from Model A in that a perfectly reflecting condition is imposed at the inlet boundary, rather than the measured reflection coefficient. The difference between Model A and Model C lies in the spatial distribution of the time delay; Model C uses a constant value of $\tau$ over the whole flame region. Furthermore, Model D assumes a thin flat flame shape with a constant value of $\tau$ at the dump plane, as illustrated in Fig. 5.

The first numerical simulation is performed with the baseline model (Model A) by varying the combustion chamber length under the Flame H00 condition. Using the comparison of the mode frequency between the measured and predicted values from Fig. 7(a), the measured pressure oscillations are identified to be in the first longitudinal (1L) mode resonating acoustically within the combustion chamber. However, the predicted frequencies are about 27% higher than the measured ones. The overprediction of resonant frequency is mainly attributed to the assumption that the burnt gas properties are distributed uniformly over the whole combustion chamber, which is not justified for the acoustically non-compact flame zone. Moreover, the speed of sound for the combustion gas is obtained with the zero-dimensional chemical equilibrium calculation, which does not consider convective and radiative heat losses or the nonequilibrium chemistry effect. In Fig. 7(b), the linear stabilities of the first three longitudinal modes are numerically analyzed in terms of the growth rate, which is the imaginary part of the complex valued angular frequency. A positive growth rate indicates that small perturbations will be amplified exponentially with time, while a negative value indicates a linearly stable condition in which pressure oscillations are damped out. As shown by the plot, only the 1L mode is expected to be excited for the chamber lengths ranging from 1.2 m to 1.9 m, while the other two modes are predicted to remain stable over the entire chamber length. In the experiment, the self-excited pressure oscillations are observed for chamber lengths ranging between 1.32 m and 1.52 m. The overestimation of the chamber length range in which the spontaneous instabilities occur could be attributed mainly to the neglect of the damping processes inherent in the system. In a real

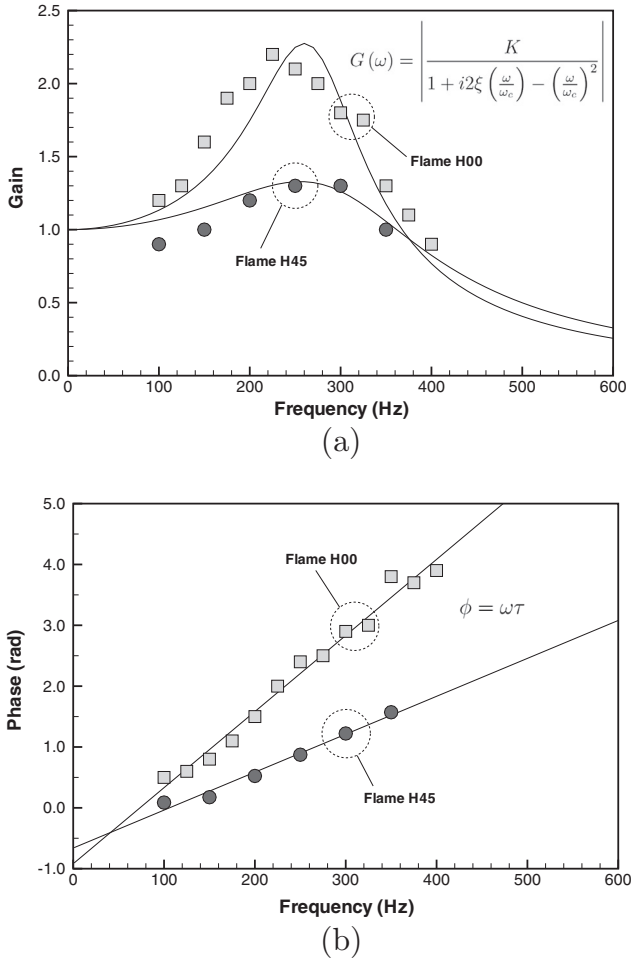


**Fig. 6.** Global flame transfer functions for the two flame conditions. (a) Gain and (b) phase (symbols: measurements [28]; lines: curve fits).

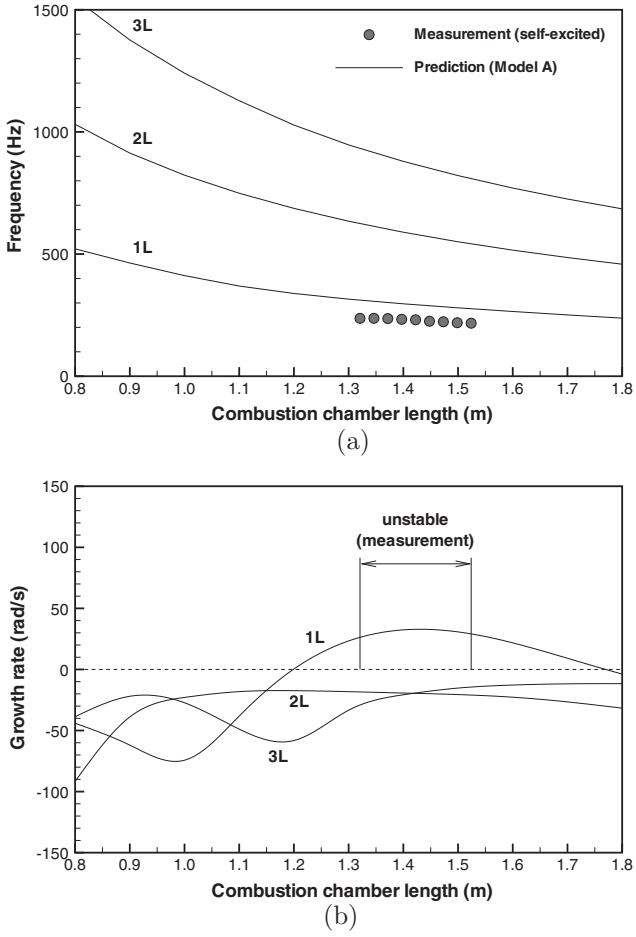


**Fig. 7.** Prediction of three longitudinal modes by varying the chamber length for Flame H00. (a) Frequency and (b) growth rate.

situation, as pointed out by Silva et al. [20], there are various physical processes which dissipate the acoustic energy and, therefore, it is necessary to judge the onset of instability only when the growth rate is greater than the overall damping rate of the system. The damping rate is difficult to quantify through measurement or numerical simulation, and no information is available for the model combustor to be analyzed in this study. Although there are the quantitative discrepancies, the numerical results show the same tendencies as the experimental results: Flame H00 is vulnerable to spontaneous combustion instability in the 1L mode for a combustion chamber length of approximately 1.42 m.

Fig. 8 presents the comparison between the predicted and measured results for Flame H45. As with Flame H00, this flame condition is predicted to exhibit self-excited pressure oscillations in the 1L acoustic mode, as shown in Fig. 8(a). Although the resonant frequencies are still overpredicted, the discrepancies between the prediction and the measurement are significantly reduced compared to those of Flame H00. This is because the relatively shortened flame zone of Flame H45 relieves the modeling defect due to the uniform distribution of gas properties within the combustion chamber. Fig. 8(b) demonstrates that the measured instabilities take place for chamber lengths ranging between 0.98 m and 1.15 m, which are substantially shorter than those of Flame H00. The numerical result predicts the instabilities for chamber lengths ranging from 0.82 m to 1.10 m. In addition, the second longitudinal (2L) mode is predicted to become unstable when the combustion chamber is longer than 1.6 m; this was not observed in the experiment. This false prediction for the 2L mode would again indicate the need to quantify system damping through further study. Overall, the Helmholtz solver qualitatively reproduces the experimental observation that the addition of $H_2$ to the natural gas fuel leads to a shorter chamber length for the self-excited instability.

Next, to examine the importance of acoustic conditions at the flow boundaries, the 1L eigenmode with a chamber length of 1.0 m and Flame H45 condition is predicted for two different inlet boundary conditions: (1) Model A with $R_{in} = 0.2292–0.1894i$, as measured [30] and (2) Model B with $R_{in} = 1$, assuming perfect

**Table 3**
Four different models for flame response and acoustic boundary treatment.

| Model | Flame shape | Time delay | $R_{in}$ | Comment |
|---|---|---|---|---|
| Model A | Actual | Linear ($\tau \pm \Delta\tau$) | 0.2292–0.1894$i$ | Baseline model |
| Model B | Actual | Linear ($\tau \pm \Delta\tau$) | 1 | Acoustic b.c. at inlet |
| Model C | Actual | Constant ($\Delta\tau = 0$) | 0.2292–0.1894$i$ | Distribution of $\tau$ |
| Model D | Thin flat | Constant ($\Delta\tau = 0$) | 0.2292–0.1894$i$ | Thin flat flame |

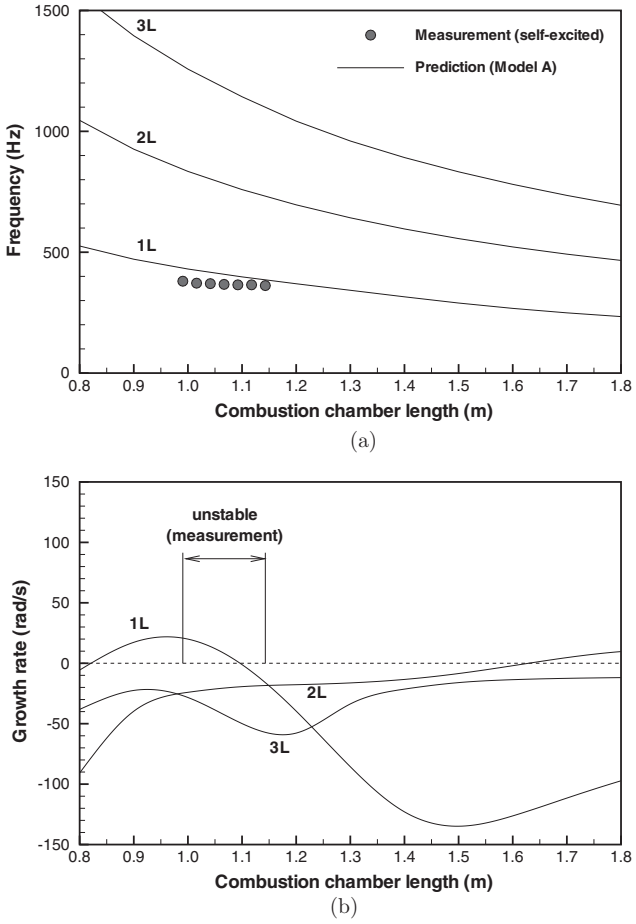


**Fig. 8.** Prediction of three longitudinal modes by varying the chamber length for Flame H45. (a) Frequency and (b) growth rate.

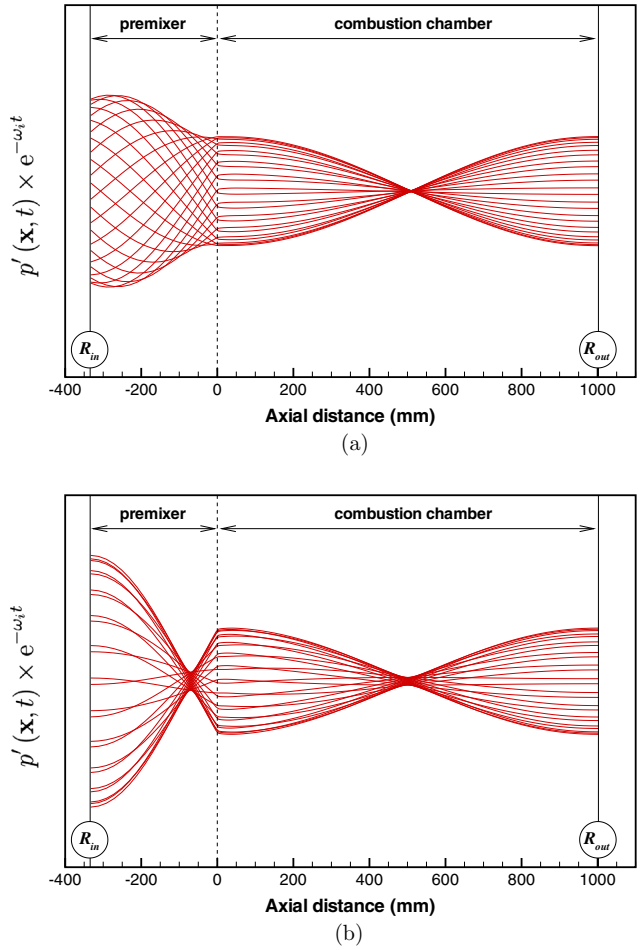


**Fig. 9.** Effect of inlet acoustic boundary condition on 1L mode shape with chamber length of 1 m for Flame H45. (a) Measured reflection coefficient ($R_{in} = 0.2292-0.1894i$); (b) Perfectly reflecting boundary ($R_{in} = 1$).

reflection of the incident wave. In the case of Model A, the finite value boundary impedance, with both resistive and reactive parts, yields acoustic radiation and phase lag at the boundary. This is reflected in the mode shape within the mixing section, as shown in Fig. 9(a). On the other hand, Model B has a homogeneous Neumann condition ($|Z| = \infty$) acting like a rigid wall. Therefore, as demonstrated in Fig. 9(b), standing wave is formed within the mixing section with pressure anti-nodes both at the inlet and at the dump plane. Fig. 10 presents the temporal evolution of pressure oscillation at the inlet. Both the models predict positive values for the growth rate, indicating exponentially increasing amplitude over time. However, Model B, with no acoustic flux at the inlet, yields more drastic growth compared to that of Model A with its inflow acoustic damping. This difference in the inlet boundary conditions is more pronounced in the numerical results of the growth rate, predicted over the whole range of the chamber length, as shown in Fig. 11. Model B, with the inadequate boundary condition, yields the false prediction that the self-excited instabilities in the 1L mode take place regardless of the chamber length. These results reaffirmed that acoustic conditions at the flow boundaries should be very carefully handled for reliable prediction of the thermoacoustic instabilities, as was extensively indicated by the previous studies [19,32].

The last part of this study aims to identify which factor plays a key role in modeling unsteady heat release in the non-compact flame zone. For Flame H00, which has the longer flame zone, the 1L eigenmodes are calculated over the whole range of the chamber length using two other flame models: (1) Model C which uses the actual flame shape and (2) Model D which assumes the thin flat flame. As shown in Fig. 12, there is no significant difference between Model C and Model D. This clearly indicates that whether the flame response with overall same sensitivity is concentrated or widely distributed has only marginal influence if a uniform distribution of time delay is assumed. Much closer agreement with the experimental observation is achieved by Model A, which has a linear profile of time delay, mimicking the local FTF measurement. These results reveal that it is crucial to appropriately model spatial distribution of time delay for the prediction of thermoacoustic instabilities induced by non-compact premixed flames.

## 4. Conclusion

This study developed an in-house Helmholtz solver by adopting the FEM on a mixed element mesh and the shift-invert method for solving the eigenvalue problem. It has been applied to simulate self-excited instabilities in a lean premixed, swirl stabilized, model gas turbine combustor with well-established measurements. The present solver, combined with the global FTF measurements, can effectively and qualitatively reproduce the instability characteristics that were experimentally observed when varying the chamber length under two different flame conditions. A comparative study has reconfirmed that the acoustic conditions at the flow boundaries have a significant impact on the longitudinal mode shapes and the acoustic loss. It has also been demonstrated that for the

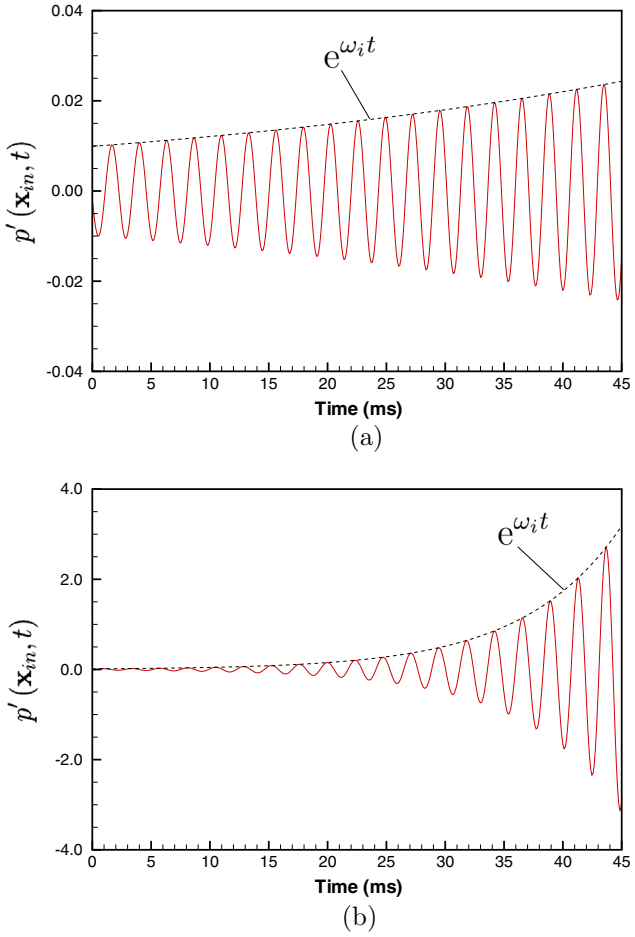


**Fig. 10.** Temporal evolution of pressure fluctuation at inlet with chamber length of 1 m for Flame H45. (a) Measured reflection coefficient ($R_{in} = 0.2292-0.1894i$); (b) Perfectly reflecting boundary ($R_{in} = 1$).

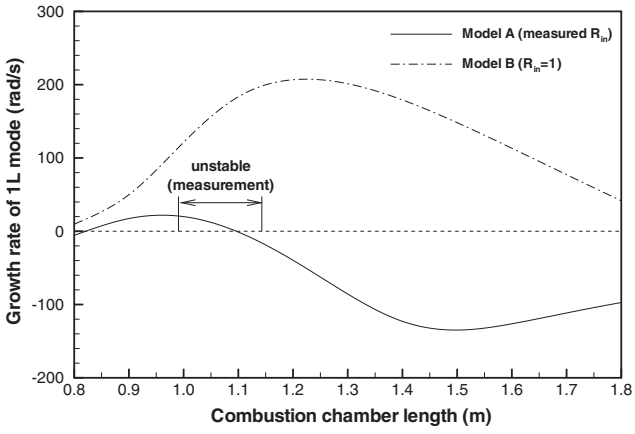


**Fig. 11.** Effect of inlet acoustic boundary condition on prediction of self-excited instability with varying chamber length for Flame H45.

prediction of combustion instabilities induced by the non-compact flame zone, it is necessary to appropriately model the spatial distribution of time delay for gain and a non-uniformity of sonic velocity within the combustion chamber for resonant frequency. Moreover, it is important to estimate the overall damping inherent in the system so that the Helmholtz solver may more accurately judge the

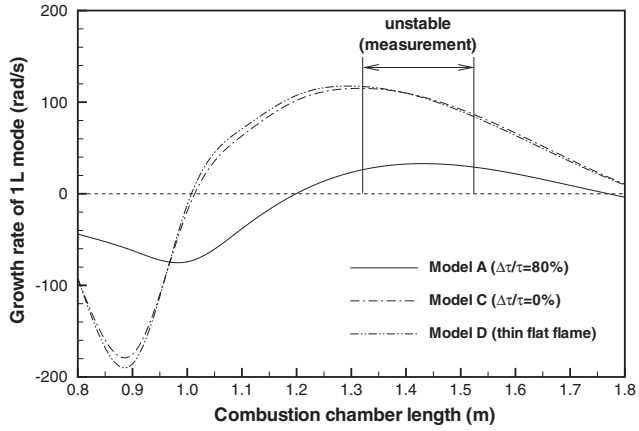


**Fig. 12.** Effect of flame response model on prediction of self-excited instability with varying chamber length for Flame H00.

occurrence of instability. These modeling issues could not be resolved solely by experimental measurement. CFD could provide complementary solutions and will be included in our future work.

## Conflict of Interest

Authors declare that there is no conflict of interest.

## Acknowledgments

The authors thank Prof. Kyu Tae Kim of KAIST for providing additional information and comments on his experimental work. The last two authors appreciate the New & Renewable Energy Core Technology Program of the Korea Institute of Energy Technology Evaluation and Planning (KETEP) for support granted financial resource from the Ministry of Trade, Industry & Energy, the Republic of Korea (No. 2011951010001C). Also, this research was supported by Basic Science Research Program through the National Research Foundation of Korea (NRF) funded by the Ministry of Education (NRF-2015R1D1A1A01058410).

## References

[1] T. Lieuwen, V. Yang, Combustion Instabilities in Gas Turbine Engines: Operational Experience, Fundamental Mechanisms, and Modeling, American Institute of Astronautics and Aeronautics, 2005.
[2] K. Zähringer, D. Durox, F. Lacas, Helmholtz behavior and transfer function of an industrial fuel swirl burner used in heating systems, Int. J. Heat Mass Transfer 46 (18) (2003) 3539–3548, https://doi.org/10.1016/S0017-9310(03)00130-3.
[3] D. Zhao, C. Ji, X. Li, S. Li, Mitigation of premixed flame-sustained thermoacoustic oscillations using an electrical heater, Int. J. Heat Mass Transfer 86 (2015) 309–318, https://doi.org/10.1016/j.ijheatmasstransfer.2015.03.012.
[4] J. O'Connor, V. Acharya, T. Lieuwen, Transverse combustion instabilities: acoustic, fluid mechanic, and flame processes, Prog. Energy Combust. Sci. 49 (2015) 1–39, https://doi.org/10.1016/j.pecs.2015.01.001.
[5] S. Candel, D. Durox, T. Schuller, P. Palies, J.F. Bourgouin, J.P. Moeck, Progress and challenges in swirling flame dynamics, Comptes Rendus Mecanique 340 (11) (2012) 758–768, https://doi.org/10.1016/j.crme.2012.10.024.
[6] T. Poinsot, Prediction and control of combustion instabilities in real engines, Proc. Combust. Inst. 36 (1) (2017) 1–28, https://doi.org/10.1016/j.proci.2016.05.007.
[7] T. Poinsot, D. Veynante, Theoretical and Numerical Combustion, second ed., R. T. Edwards Inc., 2005.
[8] L. Li, D. Zhao, X. Yang, Effect of entropy waves on transient energy growth of flow disturbances in triggering thermoacoustic instability, Int. J. Heat Mass Transfer 99 (2016) 219–233, https://doi.org/10.1016/j.ijheatmasstransfer.2016.03.084.
[9] S.R. Stow, A.P. Dowling, Thermoacoustic oscillations in an annular combustor, in: ASME Turbo Expo, 2001, Paper No. 2001-GT-0037. doi:https://doi.org/10.1115/2001-GT-0037.

[10] S. Lei, A. Turan, Chaotic modelling and control of combustion instabilities due to vaporization, Int. J. Heat Mass Transfer 53 (21-22) (2010) 4482–4494, https://doi.org/10.1016/j.ijheatmasstransfer.2010.06.045.
[11] L.Y.M. Gicquel, G. Staffelbach, T. Poinsot, Large eddy simulations of gaseous flames in gas turbine combustion chambers, Prog. Energy Combust. Sci. 38 (6) (2012) 782–817, https://doi.org/10.1016/j.pecs.2012.04.004.
[12] Y. Huang, V. Yang, Dynamics and stability of lean-premixed swirl-stabilized combustion, Prog. Energy Combust. Sci. 35 (4) (2009) 293–364, https://doi.org/10.1016/j.pecs.2009.01.002.
[13] P. Wang, N.A. Platova, J. Frohlich, U. Maas, Large Eddy Simulation of the PRECCINSTA burner, Int. J. Heat Mass Transfer 70 (2014) 486–495, https://doi.org/10.1016/j.ijheatmasstransfer.2013.11.025.
[14] F. Nicoud, L. Benoit, C. Sensiau, T. Poinsot, Acoustic modes in combustors with complex impedances and multidimensional active flames, AIAA J. 45 (2) (2007) 426–441, https://doi.org/10.2514/1.24933.
[15] C.E. Martin, L. Benoit, Y. Sommerer, F. Nicoud, T. Poinsot, Large-eddy simulation and acoustic analysis of a swirled staged turbulent combustor, AIAA J. 44 (4) (2006) 741–750, https://doi.org/10.2514/1.14689.
[16] L. Selle, L. Benoit, T. Poinsot, F. Nicoud, W. Krebs, Joint use of compressible large-eddy simulation and Helmholtz solvers for the analysis of rotating modes in an industrial swirled burner, Combust. Flame 145 (2006) 194–205, https://doi.org/10.1016/j.combustflame.2005.10.017.
[17] P. Wolf, G. Staffelbach, L.Y.M. Gicquel, J. Muller, T. Poinsot, Acoustic and large eddy simulation studies of azimuthal modes in annular combustion chambers, Combust. Flame 159 (11) (2012) 3398–3413, https://doi.org/10.1016/j.combustflame.2012.06.016.
[18] E. Gullaud, F. Nicoud, Effect of perforated plates on the acoustics of annular combustors, AIAA J. 50 (12) (2012) 2629–2642, https://doi.org/10.2514/1.J050716.
[19] C.F. Silva, I. Duran, F. Nicoud, S. Moreau, Boundary conditions for the computation of thermoacoustic modes in combustion chambers, AIAA J. 52 (6) (2014) 1180–1193, https://doi.org/10.2514/1.J052114.
[20] C.F. Silva, F. Nicoud, T. Schuller, D. Durox, S. Candel, Combining a Helmholtz solver with the flame describing function to assess combustion instability in a premixed swirled combustor, Combust. Flame 160 (9) (2013) 1743–1754, https://doi.org/10.1016/j.combustflame.2013.03.020.
[21] S.M. Camporeale, B. Fortunato, G. Campa, A finite element method for three-dimensional analysis of thermo-acoustic combustion instability, J. Eng. Gas Turb. Power 133 (1) (2010) 011506, https://doi.org/10.1115/1.4000606.
[22] D. Laera, G. Campa, S.M. Camporeale, A finite element method for a weakly nonlinear dynamic analysis and bifurcation tracking of thermo-acoustic instability in longitudinal and annular combustors, Appl. Energy 187 (2017) 216–227, https://doi.org/10.1016/j.apenergy.2016.10.124.
[23] W.C. Ullrich, C. Hirsch, T. Sattelmayer, K. Lackhove, A. Sadiki, A. Fischer, M. Staufer, Combustion noise prediction using linearized Navier-Stokes equations and large-eddy simulation sources, J. Propuls. Power, 2017, in press. doi: https://doi.org/10.2514/1.B36428.
[24] M. Schulze, T. Hummel, N. Klarmann, F. Berger, B. Schuermans, T. Sattelmayer, Linearized Euler equations for the prediction of linear high-frequency stability in gas turbine combustors, J. Eng. Gas Turb. Power 139 (3) (2017) 031510, https://doi.org/10.1115/1.4034453.
[25] M. Schulze, T. Sattelmayer, Linear stability assessment of a cryogenic rocket engine, Int. J. Spray Combust. Dyn., 2017, in press. doi:https://doi.org/10.1177/1756827717695281.
[26] S.-K. Kim, H.S. Choi, H.J. Kim, Y.S. Ko, C.H. Sohn, Finite element analysis for acoustic characteristics of combustion stabilization devices, Aerospace Sci. Technol. 42 (2015) 229–240, https://doi.org/10.1016/j.ast.2015.01.024.
[27] R. Lehoucq, D. Sorensen, ARPACK User's Guide: Solution of Large Scale Eigenvalue Problems with Implicitly Restarted Arnoldi Methods, 1997. <http://www.caam.rice.edu/software/ARPACK/>.
[28] K.T. Kim, J.G. Lee, H.J. Lee, B.D. Quay, D. Santavicca, Characterization of forced flame response of swirl-stabilized turbulent lean-premixed flames in a gas turbine combustor, J. Eng. Gas Turb. Power 132 (2010) 041502, https://doi.org/10.1115/1.3204532.
[29] K.T. Kim, H.J. Lee, J.G. Lee, B.D. Quay, D. Santavicca, Flame transfer function measurement and instability frequency prediction using a thermoacoustic model, in: ASME Turbo Expo, 2009, Paper No. GT2009-60026. doi:https://doi.org/10.1115/GT2009-60026.
[30] K.T. Kim, J.G. Lee, B.D. Quay, D. Santavicca, Spatially distributed flame transfer functions for predicting combustion dynamics in lean premixed gas turbine combustors, Combust. Flame 157 (9) (2010) 1718–1730, https://doi.org/10.1016/j.combustflame.2010.04.016.
[31] R. Kulkarni, F. Nicoud, Predicting limit cycle amplitudes by combining a Helmholtz solver with a flame describing function, in: International Summer School and Workshop on Non-Normal and Nonlinear Effects in Aero- and Thermoacoustics, Munich, May 17–21, 2010.
[32] N. Lamarque, T. Poinsot, Boundary conditions for acoustic eigenmodes computation in gas turbine combustion chambers, AIAA J. 46 (9) (2008) 2282–2292, https://doi.org/10.2514/1.35388.
[33] P.R. Amestoy, I.S. Duff, J. Koster, J.-Y. L'Excellent, A fully asynchronous multifrontal solver using distributed dynamic scheduling, SIAM J. Matrix Anal. Appl. 23 (1) (2001) 15–41, https://doi.org/10.1137/S0895479899358194.
[34] MUltifrontal Massively Parallel Solver (MUMPS 5.0.2) User's Guide, 2016. <http://mumps.enseeiht.fr/>.
[35] T. Poinsot, C.L. Chatelier, S.M. Candel, E. Esposito, Experimental determination of the reflection coefficient of a premixed flame in a duct, J. Sound Vib. 107 (2) (1986) 265–278, https://doi.org/10.1016/0022-460X(86)90237-3.
[36] W. Polifke, C. Wall, P. Moin, Partially reflecting and non-reflecting boundary conditions for simulation of compressible viscous flow, J. Comput. Phys. 203 (2006) 437–449, https://doi.org/10.1016/j.jcp.2005.08.016.
[37] C.A. Armitage, A.J. Riley, S. Cant, A.P. Dowling, S.R. Stow, Flame transfer function for swirled LPP combustion from experiments and CFD, in: ASME Turbo Expo, 2004, Paper No. GT2004-53820. doi:https://doi.org/10.1115/GT2004-53820.